

Lithographically defined uniform worm-shaped polymeric nanoparticles

This article has been downloaded from IOPscience. Please scroll down to see the full text article.

2010 Nanotechnology 21 095301

(<http://iopscience.iop.org/0957-4484/21/9/095301>)

[The Table of Contents](#) and [more related content](#) is available

Download details:

IP Address: 129.110.33.9

The article was downloaded on 13/04/2010 at 15:44

Please note that [terms and conditions apply](#).

Lithographically defined uniform worm-shaped polymeric nanoparticles

L Tao¹, X M Zhao¹, J M Gao² and W Hu^{1,3}

¹ Department of Electrical Engineering, University of Texas at Dallas, Richardson, TX 75080, USA

² Department of Pharmacology, Simmons Comprehensive Cancer Center, University of Texas Southwestern Medical Center, TX 75390, USA

E-mail: walter.hu@utdallas.edu

Received 28 October 2009, in final form 5 January 2010

Published 29 January 2010

Online at stacks.iop.org/Nano/21/095301

Abstract

We report a nanoimprint lithography method combined with photolithography on a bi-layer polymer setup to define nano-worms laterally in nano-gratings and produce uniform worm-shaped polymeric nanoparticles in aqueous solution by dissolving water soluble sacrificial layer poly(vinyl alcohol) (PVA). Process control of the thin residue layer, *SU-8* curing using broadband UV source, and warm development to remove any residue are necessary to ensure success of this technique. The use of water soluble PVA as a releasing layer and elimination of an invasive plasma etching for the releasing process makes this protocol highly compatible with biomaterials. Direct release and suspension of fluorescent worm-shaped nanoparticles (length to width ratio up to 75) in aqueous solution were demonstrated. Compared to the worm-shaped nanoparticles made by self-assembly, these lithographically defined nano-worms have much better controllability and uniformity on the shape, size, and aspect ratio. The availability of these precisely defined non-spherical particles would be important to develop a comprehensive understanding of the shape effects of nanoparticles on their efficacy in nanomedicine applications.

(Some figures in this article are in colour only in the electronic version)

1. Introduction

Nanoscale polymeric particles are of great importance as enabling nanomedicine platforms [1, 2], especially in diagnostic imaging and drug delivery applications [3–5]. Size and shape are two fundamental parameters of nanoparticles. Although the effect of particle size on the *in vivo* behavior of particulates has been well documented in the literature [6, 7], the particle shape has only recently been investigated and showed remarkably different properties over spherical particles [8–13]. For instance, disc-shaped particles exhibited higher targeting specificity to endothelial cells expressing ICAM-1 receptors in mice than spherical counterparts [10]. Rod-shaped particles shown much faster *in vitro* internalization into HeLa cells than spherical ones with the same volume [11]. Most notably, worm-shaped particles with high aspect ratio have demonstrated considerably longer blood circulation

and higher targeting efficiency [12], as well as reduced phagocytosis [13] *in vitro* compared to spherical particles with similar volumes.

Despite these promising advances, non-spherical particles have not been widely investigated to understand how the shape affects their performance in biological systems. The major roadblock on the way is the difficulty to simultaneously and precisely control the shape and size of particles with currently available methods for fabrication. Bottom-up methods, such as emulsion polymerization, mostly lead to spherical nanoparticles due to the minimization of surface energy during the fabrication process. This limitation has greatly motivated the development of new top-down lithographic methods, such as step-flash imprint lithography (S-FIL) [14, 15], soft lithography with PDMS [16] or PFPE molds (PRINT[®]) [17–19], and bi-layer nanoimprint lithography (NIL) [20]. Using these methods, short nano-rods with multi-functionality have been successfully produced in large quantities [18–20]. However, in these methods,

³ Author to whom any correspondence should be addressed.

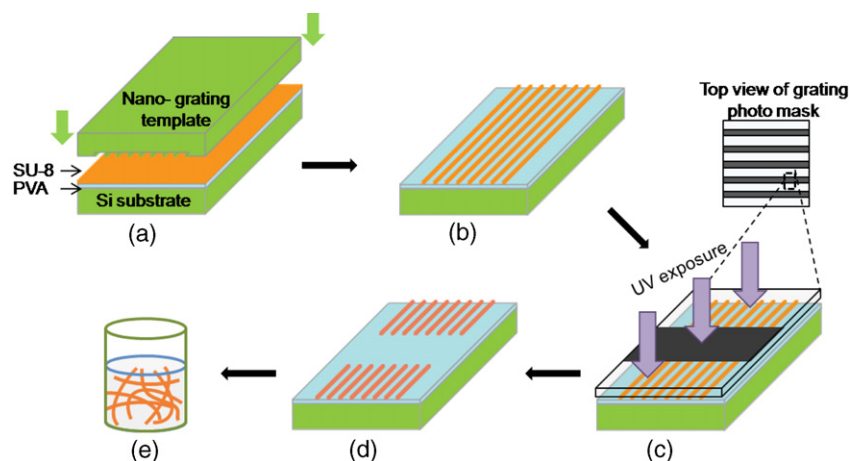


Figure 1. Schematic of the fabrication process: (a) nanoimprint on bi-layer polymer films (*SU-8* on *PVA*) spin-coated on a *Si* substrate; (b) imprinted sub-100 nm high-density *SU-8* gratings over large area; (c) UV exposure with micron grating photo-masks to cure segments of the *SU-8* nano-gratings; (d) formation of discrete cured *SU-8* nano-worms with removal of uncured *SU-8* and the ultra-thin *SU-8* residue by development; and (e) *SU-8* nano-worms were released in aqueous solution by dissolving the sacrificial *PVA* layer in water.

cylindrical polymer particles or nano-rods are typically made by vertically flowing or molding polymer into nanocavities in molds, for which the aspect ratio of nano-rods is limited to 8–9 [20]. Short nano-rods are rigid and less flexible than long worm-shaped particles that may comply with flood flow for prolonged blood circulation [12]. Although they are among the most interesting particle platforms for nanomedicine, long nano-rods or worm-shaped particles of well-controlled geometry and uniformity have not yet been demonstrated.

Here we report a lithographic approach that combines NIL with photolithography to produce worm-shaped fluorescent nanoparticles with well-controlled length, width, and uniformity. In this approach, polymeric nano-worms are defined in lateral gratings, instead of vertical pillars, to enable a high aspect ratio structure, avoiding the vertical de-molding limitation. Moreover, our process is friendly to bio-polymers because of the elimination of the invasive plasma etching step to remove any residue and the use of water soluble poly(vinyl alcohol) (*PVA*) as a sacrificial layer for releasing particles directly into aqueous solution.

2. Experimental details

Figure 1 shows the schematic of the fabrication process. A bi-layer polymer design was employed, as in our previous study [20]. UV-curable *SU-8* mixed with fluorescence dye was spin-coated on top of a sacrificial *PVA* layer. NIL was performed using a 1×1 in² template with sub-100 nm wide line grating patterns. Nanoimprinted continuous *SU-8* gratings were then selectively cured under a photomask into discrete worm-shaped particles via photolithography followed by development of *SU-8* (removing unexposed resist). The length of nano-worms is defined by the photomask. The thin *SU-8* residual layer underneath the nano-worms was removed by the developer solution, without the need of invasive plasma etching. After the *SU-8* development, nano-worms were then released from the substrate by soaking the sample in water to

dissolve the sacrificial *PVA* layer. Purification of the collected solution was done by centrifugation.

The *SU-8* composite solution was diluted from *SU-8* 2002 (Microchem[®]) with cyclopentanone at a volume ratio 1:9 doped with 0.06 wt% BODIPY[®] 493/503 fluorescence dye. The releasing/sacrificial polymer *PVA* was dissolved in distilled water at the concentration of 1 g/10 ml. The solution was purified by vacuum filtration with a 0.22 μ m Millipore Express[®] PLUS membrane. An 80 nm thick *PVA* film was spin-coated on a (100) *Si* wafer. A soft bake at 115 °C for 5 min on a hotplate was performed to remove the water in the *PVA* film. Then a layer of \sim 55 nm thick *SU-8* incorporated with fluorescent dye was spin-coated on top of the *PVA* film. It is important that the underlying *PVA* is insoluble with the solvent (cyclopentanone) for *SU-8*, so that it will stay intact during the *SU-8* spin-coating. Afterward, the bi-layer film was baked at 65 °C for 2 min on a hotplate to drive out the residual solvent. The film thickness was measured by a profiler (Veeco[®] DEKTAK VIII) and cross-checked with ellipsometry (Sentech[®] 800). In order to obtain the exposure conditions in the photolithography step, the UV absorption spectrum for *SU-8* films of varied thickness (20, 120, 500–2000 nm on a \sim 80 nm thick *PVA* on a glass substrate) were measured using UV-vis (HP[®] 845 \times).

The nanoimprint was carried out on an Obducat[®] 2.5 nanoimprinter. A silicon template (Nanonex[®]) with 85 nm wide and 95 nm deep trenches with period of 200 nm was used. The template was treated with tridecafluoro-1,1,2,2-tetrahydrooctyl trichlorosilane (FDTS) in *n*-heptane as an anti-adhesion layer. NIL was performed at 85 °C and a pressure of 4 MPa for 15 min. The imprint temperature is chosen to be 30 °C above the glass transition temperature (T_g) of *SU-8*, but below the T_g of *PVA* [21] to ensure sufficient *SU-8* flow and minimize deformation of the *PVA* layer. The template and substrate were then separated (de-molding) at a temperature below 45 °C.

Photo-masks containing periodic micron gratings with 1:1 line to space ratio were made using a Heidelberg[®] DWL66

LASER writer. The mask was aligned with micron gratings perpendicular to the nanoimprinted nano-gratings on a contact printer (Quintel[®] Q4000-6, output intensity of 18 mW cm^{-2} at the i-line, 365 nm). UV exposure (typically 20–25 s) was then performed without i-line filters, for reasons explained later. Post-exposure baking was performed at 85°C on a hotplate for a few minutes to facilitate cross-linking and reduce stress. The exposed *SU-8* patterns were developed in propylene glycol monomethyl ether acetate (PGMEA). Development at 35°C was employed, based on the study explained later, to completely remove the thin residue layer between nano-worms. The typical development time was 30 s.

The samples were then dipped in water to dissolve the PVA and release *SU-8* nano-worms in aqueous solution. The solution containing the *SU-8* nano-worms and dissolved PVA was centrifuged at 2000 rpm for 10 min and the supernatant containing PVA was removed. Nano-worms were collected and suspended in 1 ml water. 0.1 ml of this suspension was dropped on a lacy carbon film supported by a copper mesh grid for SEM imaging. Fluorescence images were taken on an Olympus[®] fluorescence microscope with the excitation wavelength around 480–500 nm.

3. Results

A representative cross-sectional and top view of the nanoimprinted *SU-8* gratings on top of the PVA-coated Si substrate is shown in figure 2(a), demonstrating the excellent pattern formation and high uniformity of the process. Since the nano-worms were defined laterally with a thin layer of *SU-8*, the nanoimprint time needed to fill the grating is reduced and the fabrication yield is high without de-molding limitations. In figure 2(a), an ultra-thin ($\sim 10 \text{ nm}$) residue layer was observed, as predicted by the volume conservation [22] on *SU-8* before and after filling into cavities on the mold. It is critical to use an appropriate thickness of initial *SU-8* in this nanoimprint process so as to reduce the residual layer. Minimization of the residue layer in this step allows us to remove it in the developer solvent and avoids the use of invasive plasma etching to create discrete nano-worms for later harvesting. Figure 2(b) shows high-density arrays (100 nm wide spacing) of cured worm-shaped nanoparticles from previously nanoimprinted *SU-8* gratings after broadband UV exposure (nominal dose 380 mJ cm^{-2} at i-line) and development (detailed discussion in section 4). The clearly shaped and waving nano-worms in figure 2(c) indicate the complete removal of *SU-8* residue between these nano-worms and the flexibility of these high aspect ratio *SU-8* worms. These lithographically defined nano-worms show excellent uniformity in their dimension and shape in comparison to those made by conventional solution chemistry based fabrication [12, 23]. The curvature of these *SU-8* worms is caused by the solution-induced stress [24, 25] during the *SU-8* development process. The flexibility of *SU-8* worms could be controlled by the degree of cross-linking or UV exposure dose.

The well-defined worm-shaped nanoparticles were released from substrate to aqueous solution by dissolving the underlayer PVA layer in water. Figure 3(a) shows a single worm-shaped nanoparticle of 80 nm in width (diameter) and $6 \mu\text{m}$

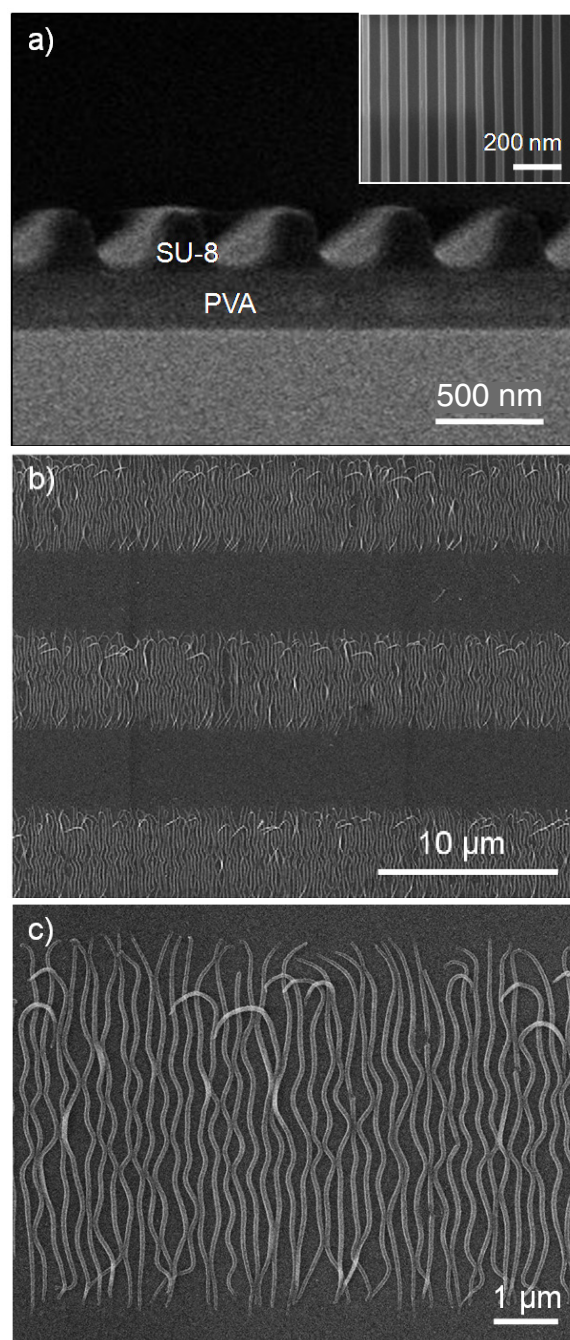


Figure 2. SEM images of (a) nanoimprinted $\sim 85 \text{ nm}$ wide and $\sim 90 \text{ nm}$ tall line gratings with an ultra-thin *SU-8* residue layer ($\sim 10 \text{ nm}$) on top of PVA (inset: top view); (b) $6 \mu\text{m}$ long (aspect ratio 75) nano-worms formed by chopping the gratings via photolithography and development; (c) zoomed-in view of free nano-worms showing excellent uniformity and some degree of flexibility.

in length (length to width ratio 75), collected from the releasing aqueous solution. By varying the grating width on the photomask, nano-worms with different lengths can be easily achieved with excellent uniformity and flexibility. Fabrication and releasing of a large amount of these uniform nano-worms had been demonstrated, as shown in figure 3(b). The throughput of this process is on the order of 10^8 nano-worms per in^2 .

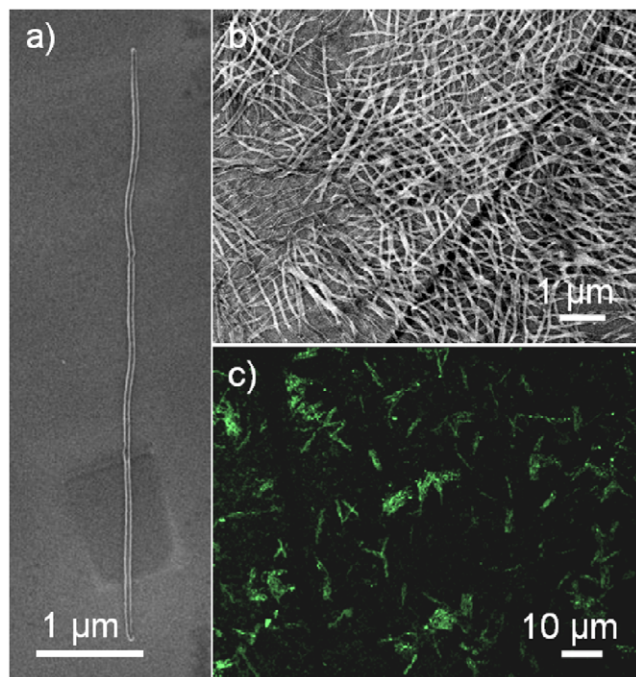


Figure 3. SEM images of released (a) single and (b) large amounts of *SU-8* nano-worms of 80 nm in width, 6 μm in length (aspect ratio of 75), collected from aqueous solution after releasing them into water. (c) Fluorescent image of free *SU-8* nano-worms collected from aqueous solution.

The direct releasing of particles into aqueous solution by dissolving water soluble PVA improves the compatibility of this fabrication process for use with bio-polymers in the future in comparison to the use of acetone in harvesting [18, 20]. In figure 3(c), the fluorescent image of the released nano-worms illustrates the preserved functionality of BODIPY[®] dye encapsulated in the *SU-8* nano-worms. Other agents such as superparamagnetic iron oxide (SPIO) for MRI imaging can also be incorporated in *SU-8* (results not shown). The capability of incorporating various bio-agents into these nano-worms is needed for multi-functionality in nanomedicine applications.

4. Discussions

Making polymeric nano-worms requires patterning of particles with ultra-high aspect ratio (length to width >20). This is difficult to achieve for previously reported NIL processes where nano-rods were defined vertically [15, 17, 20]. For these methods, there would be a limitation on the highest aspect ratio achievable by the vertical de-molding process, as indicated by the following theoretical analysis of the de-molding process. Taking cylindrical *SU-8* rods as an example (figure 4(a)), the requirement for successful separation of *SU-8* patterns from the mold without breaking is that the adhesion energy (W_{mp}^a) between the rods and mold should be less than the *SU-8* cohesion energy (W_p^c). W_{mp}^a can be estimated as the sum of *SU-8*-mold adhesion and dynamic friction between the *SU-8* and the side wall of mold cavities (equation (1)). The mold-*SU-8* adhesion energy is defined with equation (2) [26],

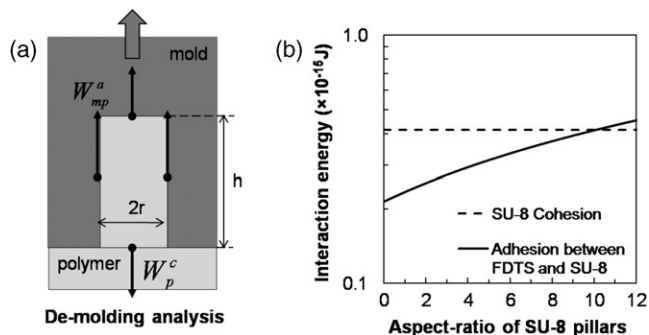


Figure 4. (a) Model of de-molding process in nanoimprint lithography and (b) calculated cohesion energy of *SU-8* pillars and their adhesion with the mold as a function of the aspect ratio of the nano-pillars.

where γ^p and γ^d are the polar and dispersive surface energies of each substance, which are measured using a two-liquid method [26]. The measured surface energies of *SU-8* and FDTs treated Si surfaces are 41.2 mJ m⁻² ($\gamma^p = 4.0$ mJ m⁻², $\gamma^d = 37.2$ mJ m⁻²) and 15 mJ m⁻² ($\gamma^p = 2.8$ mJ m⁻², $\gamma^d = 12.2$ mJ m⁻²) respectively, in agreement with reported values [27]. The cohesion energy of the *SU-8*, W_p^c , is calculated in equation (3). The dynamic friction (μ_d) is estimated as ~0.05 [28, 29]. W_{mp}^a and W_p^c are then calculated and plotted as a function of the aspect ratio (height h over diameter $2r$) of *SU-8* rods, as shown in figure 4(b). The intersection of W_{mp}^a and W_p^c is the maximum aspect ratio allowable by vertical de-molding, which is found to be 9–10 and matches well with the experimental observations [20].

$$W_{mp}^a \cong \gamma_{mp}(\pi r^2 + \mu_d \pi 2rh) \quad (1)$$

$$\gamma_{mp} \cong \sqrt{\gamma_m^p \gamma_p^p} + \sqrt{\gamma_m^d \gamma_p^d} \quad (2)$$

$$W_p^c = 2\gamma_p \pi r^2. \quad (3)$$

The conclusion of this simple model is that conventional nanoimprint with vertical pillar formation cannot allow high aspect ratio (>10) pillars to survive the de-molding process. This de-molding limitation can be avoided by defining nano-worms laterally, as shown in this work. The vertical aspect ratio of the nano-worms here is only 1:1, which has enabled high nanoimprint uniformity and nearly 100% yield. One drawback of this approach is that it lowers the particle density compared to the vertically defined nanoscale structures.

As shown earlier, photolithography was used to define the lengths (2–10 μm) of nano-worms from the nanoimprinted *SU-8* gratings. Interestingly, these gratings formed from thin film (<100 nm) were difficult to cross-link using filtered i-line UV light ($\lambda = 365$ nm, Karl Suss[®] MA6 contact aligner), even with very high doses, whereas they were effectively cured under an unfiltered mercury arc lamp with a broad spectrum (output peaks at 297–302, 312–313 and 334 nm [30]). This indicates the optical property of *SU-8* films may change as the thickness decreases. To understand this phenomenon, we have measured the UV absorbance of *SU-8* films with varied thickness from nanoscale to microscale, as shown in figure 5

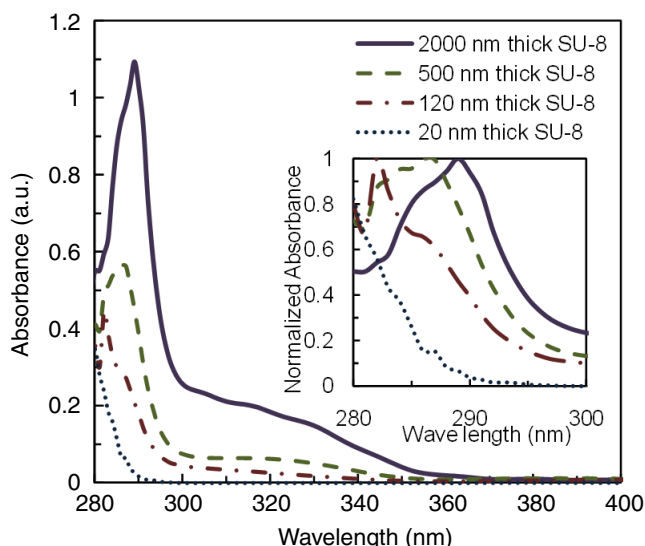


Figure 5. UV absorbance of thin *SU-8* films with different thicknesses. The inset is a zoom in plot at (280–300 nm) within the deep UV region, showing the blue shift of absorbance.

(normalized absorbance curves shown in the inset). We clearly see the blue shift of optical absorbance peaks as the thickness of *SU-8* reduces. Such a blue shift of the absorbance peak indicates the increase in the optical band gap as the thickness of *SU-8* decreases, which is in concert with the reported decrease of refractive index for thin *SU-8* films [31]. The increase of optical band gap can be attributed to the increase of unsaturated or dangling bonds in the *SU-8* resin that are produced by incomplete polymerization/cross-linking of *SU-8* as a result of an insufficient number of precursors in the thin films of high surface to volume ratio [31]. A similar observation and explanation of the blue shift of the absorbance edges in organic thin films of thiosemicarbazone was reported earlier [32].

The broadband UV source used in our experiments contains deeper UV light (280–310 nm) that can be effectively absorbed even for the thin *SU-8*. At the molecular level, the strong absorption of deep UV may be from aromatic entities and photoinitiators. As *SU-8* is a chemical amplified resist, opening of epoxy rings in *SU-8* is not usually caused by direct UV absorption but by the Lewis acids released from photoinitiators activated by UV radiation and further driven by a thermal process. Therefore, the successful curing of thin *SU-8* films attributes to the effective activation of photoinitiators by the broadband UV exposure, which results from a significant spectrum overlap of the absorbance peak (280–340 nm) of the *SU-8* photoinitiator triarylsulfonium/hexafluorophosphate [33] with the output spectrum of the unfiltered mercury lamp. It is worth noting that the use of deep UV for curing ultra-thin *SU-8* films here is quite different from the patterning of thick *SU-8* films in micro-electronic-mechanical (MEMs) applications, for which 350–400 nm UV is recommended as a tradeoff between cure efficiency and good transparency to achieve uniform cross-linking throughout the thick film [34].

Moreover, the temperature of *SU-8* development has shown a considerable effect on the formation of discrete nano-

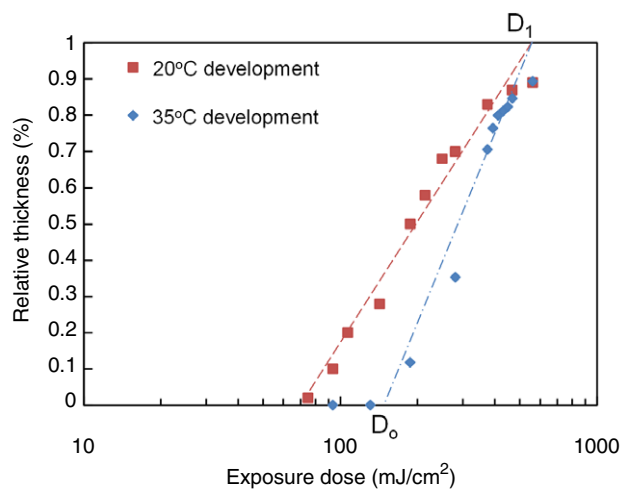


Figure 6. Remaining thickness (%) of *SU-8* at different exposure doses after 30 s development at room temperature (20 °C) and 35 °C. Development contrast ($\gamma = 1/\log(D_1/D_0)$) at 20 °C and 35 °C are ~ 1.2 and ~ 1.9 , respectively.

worms and the removal of the residue layer. If developed at room temperature (20 °C), a thin residue in *SU-8* formed by the nanoimprinting process would remain on top of PVA, leading to connected nano-worms. However, if the development temperature is elevated to 35 °C, the *SU-8* residue can be completely removed and form discrete nano-worms, as shown in figure 2(c). This phenomenon could be explained with the use of a resist contrast curve. First, to obtain the contrast curves of *SU-8* development, two groups of *SU-8* samples with the same initial thickness (85 nm) were exposed with an array of squares with gradient doses but developed at two different temperatures (20 and 35 °C) for 30 s. The remaining thicknesses for the squares under different doses for each group were measured and plotted versus exposure doses, as shown in figure 6. The contrast of resist can be calculated by $\Gamma = 1/\log(D_1/D_0)$, where D_1 and D_0 are the extrapolation of the linear portion of each curve in figure 6 to 100% (all *SU-8* is cured) and 0% (no *SU-8* is cured), respectively. The contrast curves of 35 °C development (blue curve) have a sharper slope, resulting in higher contrast ($\Gamma = 1.9$) than those of 20 °C development (red curve) ($\Gamma = 1.2$). *SU-8* developed at increased temperature (35 °C) enhanced the contrast and quality of nano-worms. This warm development method was employed to ensure the complete removal of the *SU-8* residue layer and avoid the use of the invasive plasma etching step usually employed in conventional imprint such as S-FIL [15]. In terms of material biocompatibility, *SU-8* is widely used in bio-MEMs and implantable bio-devices without any toxicity issues. However, *SU-8* may not be a good material for polymeric carriers for nanomedicine applications. The technique reported here would be highly applicable to biocompatible polymers such as polyethylene glycol and also for incorporation of bio-agents, since this nanoimprint based process eliminates the use of invasive solvents or etching steps and uses water to harvest the particles.

5. Conclusions

In summary, a nanoimprint lithography method associated with optimized photolithography and bi-layer polymer setup has been developed to produce uniform worm-shaped polymeric nanoparticles. This 'lying-down' approach enables the fabrication of nanoparticles with ultra-high length to width ratio thus avoiding the limitations of vertical de-molding in the conventional nanoimprint process. The engineering control and process optimization of the thin residue layer, SU-8 curing using a broadband UV source, and warm development to remove the residue are necessary to ensure success of this technique. Together with the use of water soluble PVA as a releasing layer, this method eliminates the need of an invasive plasma etching process. Direct release and suspension of fluorescent worm-shaped nanoparticles in aqueous solution were demonstrated. Compared to the worm-shaped nanoparticles made by self-assembly, these lithographically defined nano-worms have much better controllability and uniformity on their shape, size, and aspect ratio. The throughput of this process is 10^7 – 10^8 nanoparticles cm^{-2} area per run. We believe the availability of these precisely defined non-spherical particles would be highly important to establish a comprehensive understanding of the shape effects of nanoparticles on their *in vivo* behavior for many nanobiology and nanomedicine applications.

Acknowledgments

This work is supported by the Moncrief Foundation. The authors thank Drs Fatih Buyukserin, Ruhai Tian, and Bo Zhou in our group for helpful discussions, as well as Jing Yu and Professor Zheng Jie in the Department of Chemistry at University of Texas at Dallas for the access to the fluorescence microscope.

References

- [1] Freitas J R A 2005 *Nanomed.: Nanotechnol. Biol. Med.* **1** 2–9
- [2] Moghimi S M, Hunter A C and Murray J C 2005 *FASEB J.* **19** 311–30
- [3] Langer R 1990 *Science* **249** 1527–33
- [4] Langer R 1998 *Nature* **392** 5
- [5] Goldberg M, Langer R and Jia X 2007 *J. Biomater. Sci., Polym. Edn* **18** 241–68
- [6] Gref R, Minamitake Y, Peracchia M T, Trubetskoy V, Torchilin V and Langer R 1994 *Science* **263** 1600–3
- [7] Alexis F, Pridgen E, Molnar L K and Farokhzad O C 2008 *Mol. Pharmaceut.* **5** 505–15
- [8] Mitragotri S 2009 *Pharmaceut. Res.* **26** 488
- [9] Champion J A, Katare Y K and Mitragotri S 2007 *J. Control. Release* **121** 3–9
- [10] Muro S, Garnacho C, Champion J A, Leferovich J, Gajewski C, Schuchman E H, Mitragotri S and Muzykantov V R 2008 *Mol. Ther.* **16** 1450–8
- [11] Gratton S E A, Ropp P A, Pohlhaus P D, Luft J C, Madden V J, Napier M E and DeSimone J M 2008 *Proc. Natl Acad. Sci.* **105** 11613–8
- [12] Geng Y, Dalhaimer P, Cai S, Tsai R, Tewari M, Minko T and Discher D E 2007 *Nat. Nanotechnol.* **2** 249–55
- [13] Champion J A and Mitragotri S 2006 *Proc. Natl Acad. Sci. USA* **103** 4930–4
- [14] Colburn M et al 1999 *Proc. SPIE* **3676** 379–89
- [15] Glangchai L C, Caldorera-Moore M, Shi L and Roy K 2008 *J. Control. Release* **125** 263–72
- [16] Xia Y and Whitesides G M 1998 *Angew. Chem. Int. Edn* **37** 550–75
- [17] Rolland J P, Hagberg E C, Denison G M, Carter K R and Simone J M D 2004 *Angew. Chem. Int. Edn* **43** 5709
- [18] Gratton S E A, Pohlhaus P D, Lee J, Guo J, Cho M J and DeSimone J M 2007 *J. Control. Release* **121** 10–8
- [19] Kelly J Y and DeSimone J M 2008 *J. Am. Chem. Soc.* **130** 5438–9
- [20] Buyukserin F, Aryal M, Gao J and Hu W 2009 *Small* **5** 1632–6
- [21] Sarti B and Scandola M 1995 *Biomaterials* **16** 785–92
- [22] Lee H-J, Ro H W, Soles C L, Jones R L, Lin E K, Wu W-I and Hines D R 2005 *J. Vac. Sci. Technol. B* **23** 3023–7
- [23] Ji-Ho P, von Geoffrey M, Lianglin Z, Michael P S, Erkki R, Sangeeta N B and Michael J S 2008 *Adv. Mater.* **20** 1630–5
- [24] Huang X, Bazan G, Hill D A and Bernstein G H 1992 *J. Electrochem. Soc.* **139** 2952–6
- [25] Yoshimoto K, Stoykovich M P, Cao H B, de Pablo J J, Nealey P F and Drugan W J 2004 *J. Appl. Phys.* **96** 1857–65
- [26] Owens D K and Wendt R C 1969 *J. Appl. Polym. Sci.* **13** 1741–7
- [27] Hu W, Yang B, Peng C and Pang S W 2006 *J. Vac. Sci. Technol. B* **24** 2225–9
- [28] Romig A D, Dugger M T and McWhorter P J 2003 *Acta Mater.* **51** 5837–66
- [29] Cichomski M, Grobelny J and Celichowski G 2008 *Appl. Surf. Sci.* **254** 4273–8
- [30] Kim S-J, Yang H, Kim K, Lim Y T and Pyo H-B 2006 *Electrophoresis* **27** 3284–96
- [31] Parida O P and Bhat N 2009 Characterization of Optical Properties of SU-8 and Fabrication of Optical Components *Int. Conf. Optics and Photonics* (Chandigarh: CSIO) PS3.E.8
- [32] Yakuphanoglu F, Sekerci M and Balaban A 2004 *Opt. Mater.* **27** 1369–72
- [33] Crivello J V and Lam J H W 1980 *J. Polym. Sci.: Polym. Chem. Edn* **18** 2697–714
- [34] Williams J D and Wang W 2004 *J. Microlithogr. Microfabr. Microsyst.* **3** 563–8

Corrigendum

Lithographically defined uniform worm-shaped polymeric nanoparticles

J L Tao, X M Zhao, J M Gao and W Hu

2010 *Nanotechnology* **21** 095301

There was an error in the final published version of figure 2 (a). The scale bars for the figure and the inset have been reversed. The corrected version of figure 2 (a) is provided below.

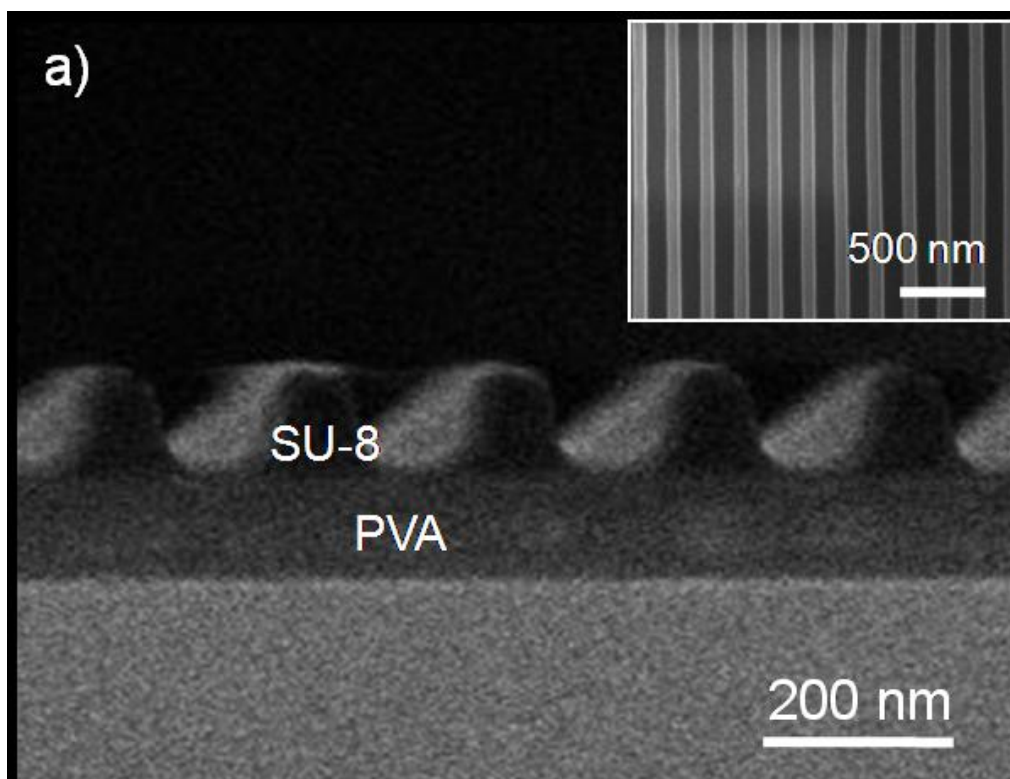


Figure 2. (a) SEM image of a nanoimprinted ~ 85 nm wide and ~ 90 nm tall line gratings with an ultra-thin SU-8 residue layer (~ 10 nm) on top of PVA (inset: top view).